Journal of Colloid and Interface Science 361 (2011) 381–387

Contents lists available at ScienceDirect

Journal of Colloid and Interface Science

www.elsevier.com/locate/jcis

Ambient pressure effects on the electrokinetic potential of Zeonor–water interfaces

Vishal Tandon [a], Brian J. Kirby [b,*]

[a] Department of Biomedical Engineering, Cornell University, United States
[b] Sibley School of Mechanical and Aerospace Engineering, Cornell University, United States

ARTICLE INFO

Article history:
Received 17 March 2011
Accepted 13 May 2011
Available online 25 May 2011

Keywords:
Hydrophobic
Electrokinetic potential
Zeta potential
Microfluidic
Nanobubble
Hysteresis
Electroosmosis
Electrophoresis
Electroosmotic mobility
Electrophoretic mobility
Cyclic olefin copolymer

ABSTRACT

Using phase-sensitive streaming potential experiments in a vacuum chamber, we demonstrate that lowering the ambient pressure of the air surrounding a hydrophobic, Zeonor microfluidic substrate results in a decrease in the time scale required for equilibration of the electrokinetic potential. At ambient air pressures below 0.74 atm, the electrokinetic potential changes from ∼−84 mV to ∼−11 mV in 5 h, while the same decrease occurs in a period of over 200 h when the system is at 1 atm. Returning a sub-atmospheric system (where the electrokinetic potential had equilibrated to −11 mV) to atmospheric pressure did not result in any additional change in the electrokinetic potential. This can be described as a type of hysteresis of the electrokinetic potential with dissolved gas concentration. No time or pressure dependence was observed for the electrokinetic potential of hydrophilic (silica) substrates.

1. Introduction

Polymers are often used as substrates for microfluidic systems, as they are inexpensive, relatively easy to fabricate, and have potential for favorable biological, chemical, and optical properties [1–4]. Modeling electrokinetics in polymeric substrates is challenging, however, because many of them are hydrophobic, and interfacial phenomena in water–hydrophobe systems are not well understood. While significant electrokinetic potentials have been observed in hydrophobic substrates [1,5–10], and at other hydrophobic interfaces such as oil droplets in water [11–15], some have reported the electrokinetic potential in those substrates to be immeasurable or unpredictable [16–18]. The lack of understanding of water–hydrophobe interfaces [10] limits predictive capabilities for device design, and can lead to inaccurate analytical results.

The complexity of hydrophobic interfaces arises from poorly defined chemical, electrical, and fluid velocity boundary conditions; the origin of charge is unknown, and there is uncertainty regarding slip [19,20]. Furthermore, these phenomena are dependent on the structure of water and the putative presence of gas at the fluid–solid interface. Regions of depleted water density [21–23], ice-like hydrogen-bonded water molecule networks [24,21,25], and nanobubbles [26] have been postulated as interfacial structures. In particular, the presence of interfacial nanobubbles would affect both surface charge and slip, and their thermodynamic instability [27,28,26,29,19] has been proposed as a potential explanation for the variation of electrokinetic properties of hydrophobic substrates as a function of the time history of the fluid–solid interface [30]. Both slip [31] and nanobubbles [32–36] have been shown to depend on the type and amount of gas dissolved in solution. This suggests that the electrokinetic properties of hydrophobic substrates also depend on dissolved gas concentration, which is a function of the ambient pressure and temperature.

Here we use phase-sensitive streaming potential experiments to measure the electrokinetic properties of hydrophobic substrates surrounded by air at sub-atmospheric pressures. Results are compared to measurements at atmospheric pressure, which are carried out to long times (200 h) in order to estimate equilibrium properties. Hydrophilic substrates (silica) are also measured for comparison. Our goal is to determine how the ambient pressure of air in contact with a water–Zeonor system affects both the equilibrium electrokinetic potential and the kinetics that govern the approach to equilibrium. This data is expected to elucidate whether the state of dissolved gases in solution is a critical parameter in these systems, and may ultimately be used to help inform design of microfluidic devices from hydrophobic polymers.

2. Reagents and substrates

Reagents were purchased from Sigma–Aldrich (St. Louis, MO). Phosphate buffer solutions were prepared from stock solutions of

* Corresponding author.
E-mail address: kirby@cornell.edu (B.J. Kirby).

0021-9797/$ - see front matter © 2011 Elsevier Inc. All rights reserved.
doi:10.1016/j.jcis.2011.05.053

monobasic and dibasic potassium phosphate. A mixture of equal parts 0.5 mM monobasic potassium phosphate and 0.5 mM dibasic potassium phosphate was used as the working solution for all experiments (pH = 7.1, $pC = -\log C = 2.8$, where C is the molar counterion concentration, consisting of potassium and hydrogen ions in this case). A dual pH/conductivity meter (Mettler Toledo SevenMulti, Columbus, OH) with specialized electrodes (Mettler Toledo Inlab 730 and Inlab 413, Columbus, OH) was used for solution conductivity and pH measurements. Prior to each experiment, buffers were checked to ensure that there were no pH or conductivity changes over time. Solution oxygen content was measured using an electrochemical dissolved oxygen sensor (PASCO PS–2108, Roseville, CA). Oxygen content was used to estimate overall dissolved gas content, relative to the dissolved O_2 concentration at atmospheric pressure (O_2 is about twice as soluble in water at room temperature as N_2 [37], and both gases have nearly the same diffusivity [38,39]). All buffers were at room temperature (T = 25 °C) for all experiments.

Silica capillaries were purchased from Polymicro Technologies Inc. (Phoenix, AZ) and Zeonor capillaries were purchased from Paradigm Optics (Vancouver, WA). The silica capillaries had outer and inner diameters of 360 μm and 25 μm, while the Zeonor capillaries had outer and inner diameters of 300 μm and 30 μm. A fresh section of capillary was used in each trial of each experiment.

3. Streaming potential measurements

Phase-sensitive streaming potential experiments (Fig. 1) were used to measure the electrokinetic potential of silica and Zeonor capillaries as a function of time [10,30]. Pressure was applied to the inlet of a 4-cm section of capillary composed of the material under study using a push/pull syringe pump (KD Scientific, Holliston, MA). Sinusoidal pressure waveforms with 240-s periods were established via PID control of syringe actuation realized by LabView. Pressure at the capillary inlet was measured by a strain-gauge transducer (Senso-Metrics SP70D, Simi Valley, CA). PEEK–ULTEM fittings (LabSmith, Livermore, CA) and 180-μm ID stainless steel tubing were used to make the fluid connections between the syringe, capillary, electrodes, and pressure transducer [40]. Leaks in the fluidic connections could lead to an underestimate of the electrokinetic potential. However, because we measured the pressure directly at the capillary inlet, and because all of the fixtures upstream of the capillary had relatively small hydraulic resistance (~3 orders of magnitude less than the capillary itself), only leaks at the capillary inlet could have potentially introduced error. We rejected data from any experiments where such leaks were observed.

A 10 TΩ electrometer (6514 Electrometer, Keithley, Cleveland, OH) along with platinized platinum electrodes were used to measure the generated voltage across the capillary. They were fabricated using an electrochemical reaction as described previously [41]. The platinizing solution consisted of 3.5% w/v hydrogen hexachloroplatinate, 0.005% w/v lead acetate, and 2.5% v/v 1M HCl solution. The working platinum electrode was immersed in the platinizing solution against a counter electrode, and a potential of 7 V was applied for 120 s, resulting in a macroscopically black (platinized) platinum electrode. Electrodes were visually inspected in order to check for degradation prior to each experiment.

For experiments at atmospheric pressure, pressure was applied to drive fluid from a syringe through the capillary under test into a reservoir. The pressure waveform ($\Delta P = P_{\text{inlet}} - P_{\text{reservoir}}$) varied from 0 to 27.6 kPa. Sub-atmospheric pressure experiments were conducted inside a vacuum oven (VWR 1430M, Radnor, PA). Pressure was applied by a syringe pump situated outside of the oven, and was transferred from the syringe pump to a syringe in the oven via a linear positioner (Huntington Mechanical Laboratories L2121–6–A, Grass Valley, CA). Electrical signals were transferred into and out of the experimental vacuum chamber using an electrical feedthrough (Huntington Mechanical Laboratories P–22328–CF, Grass Valley, CA). For these experiments, negative pressure was applied by the syringe pump at the capillary inlet so as to move fluid in the opposite direction as in the experiments at atmospheric pressure. The fluid from a large (20 ml) reservoir that was open to the local atmosphere moved through the capillary under test into a syringe. This ensured that the fluid in the capillary had been exposed to the local atmosphere, allowing for adequate gas transfer between the fluid and the air. In those experiments, the pressure difference between the inlet and the reservoir varied from −41.4 to −13.8 kPa. The flow was laminar in all cases (Reynolds number below 1200), and hydrodynamic starting lengths could be ignored. Electrical signals (i.e. the streaming potential and pressure waveforms) were sampled by a DAQ card at 20 kHz, and averaged over a period of 200 ms.

The measured pressure and streaming potential waveforms were Fourier processed in 12-min segments, and the response at

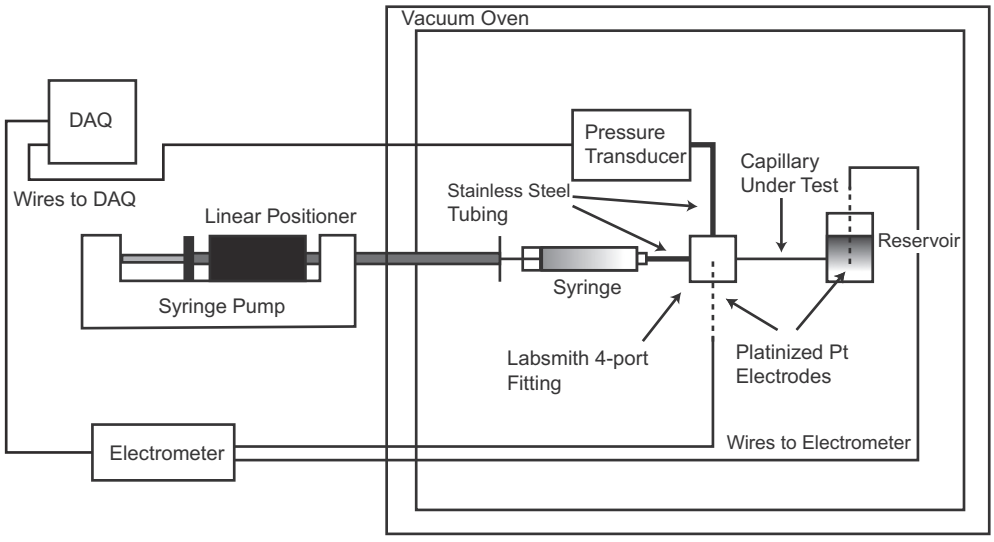

Fig. 1. Scheme of experimental setup for phase-sensitive streaming potential measurements at sub-atmospheric ambient pressures.

the fundamental mode was used to calculate the electrokinetic potential as a function of time. The electrokinetic potential was calculated from the Smoluchowski Equation as follows:

$$|\zeta| = \frac{\eta\sigma}{\epsilon}\left(\frac{|\mathcal{F}\{\phi(t)\}|}{|\mathcal{F}\{\Delta P(t)\}|}\right)\Bigg|_{f=f_0}, \quad (1)$$

where $\mathcal{F}$ denotes the discrete Fourier transform, and f_o is the driving frequency of the pressure waveform [42,10,30,43]. Errors due to surface conductivity, non-Debye–Hückel charge distributions, and wall curvature were ignored as they were small as compared to conductivity and temperature uncertainties, which were of the order of 2–3%. Given the measurement uncertainties in our system, we estimate the error in the inferred electrokinetic potential to be less than 3%, and it is primarily due to uncertainty in the solution conductivity. Because Eq. (1) holds strictly at equilibrium, the period of the applied pressure waveform was chosen to be slow enough (240 s) to allow for a quasi-static measurement. If the system does not reach equilibrium, there is a phase lag between the streaming-potential waveform and the pressure waveform. The damping of the streaming potential waveform magnitude that occurs in a system with a phase lag can be corrected for if the phase lag is measured simultaneously:

$$\zeta = \zeta_0(1 + \tan^2\alpha), \quad (2)$$

where ζ_0 is the uncorrected electrokinetic potential, and $\alpha = \angle\mathcal{F}(\phi) - \angle\mathcal{F}(\Delta P)$ is the phase difference between the streaming potential and pressure waveforms. The phase lag, however, was negligible in all of our experiments.

In order to compare experiments conducted with solutions of different ionic strengths, we normalize our electrokinetic potential data by $pC = -\log C$, where C is the counterion concentration in mol/L, as described in [44].

4. Results and discussion

4.1. Time dependence of the ζ potential at reduced ambient pressure

We used phase-sensitive streaming potential experiments to measure the electrokinetic potential of Zeonor microchannels as a function of time at ambient pressures of 1 atm, 0.87 atm, 0.74 atm, and 0.47 atm. In these experiments, Zeonor microchannels were filled with aqueous working solution and sealed inside a vacuum-oven chamber. At this point, all of the working solution in the system was at equilibrium with air at atmospheric pressure and room temperature. The pressure was then lowered to the desired value using a mechanical pump, and simultaneous sinusoidal pressure actuation and streaming potential measurement were initiated immediately thereafter. The specified sub-atmospheric pressures were maintained throughout the duration of each experiment. As a test case for a hydrophilic substrate, this experiment was also run for silica in air at 0.47 atm.

At all pressures, the normalized electrokinetic potential in Zeonor was initially large in magnitude at ∼−30 mV, but decayed to a smaller magnitude over time (Fig. 2). The temporal variations in the electrokinetic potential can be described as exponential decays with one or more time constants (this is discussed further in the next section). At the end of the 20 h period in which the experiments were run, the electrokinetic potential was smaller in magnitude at lower ambient pressures (Table 1). This suggests that pressure affects the equilibrium state of the electrokinetic potential and/or the kinetics of the approach toward equilibrium. This change was not caused by an increase in solution conductivity due to evaporation, as the conductivity increased by less than 3% in all experiments. The data at 0.47, 0.74, and 0.87 atm all decay to the same ζ potential at the end of the 20-h period, though it is not clear from this experiment whether the system at 1 atm would have reached the same electrokinetic potential at times greater than 20 h (see next section). For these experimental conditions, the pressure dependence is weaker below 0.47 atm, as the electrokinetic-potential traces for 0.74 atm and 0.47 atm were nearly identical.

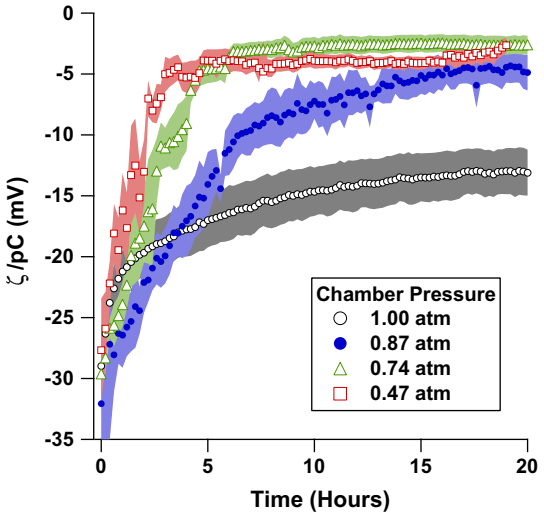

Fig. 2. Comparison of ζ-potential measurements in Zeonor at 1 atm to those at lower ambient pressures. Data shown is the electrokinetic potential, ζ, normalized by $pC = -\log C$ (C is the counterion concentration in M) as a function of time for a Zeonor substrate. 1 mM, pH 7 phosphate buffer was the working solution. The experiment was set up with all solutions in equilibrium with air at atmospheric pressure, the pressure was lowered to the indicated values, and the measurement immediately initiated thereafter. All data shown represents the mean of at least four replicates, where the shaded areas represent the standard error of the mean. One point from one trial of the 0.74 atm data, and two points from one trial of the 0.47 atm data were determined to be statistical outliers by Chauvenet's criterion, and removed (there were 101 total time points for each replicate of each pressure condition).

Table 1
Summary of results.

Pressure (atm)	$\frac{\zeta}{pC}$ (mV) at $t = 0$	$\frac{\zeta}{pC}$ (mV) at $t = 20$ h
0.47	−27.7	−2.6
0.74	−29.6	−2.6
0.87	−32.1	−4.9
1.00	−28.9	−13.1

The measured electrokinetic potential as a function of time for Zeonor at atmospheric pressure agrees well with previously reported results for TOPAS [30], a thermoplastic that is chemically similar to Zeonor, but is manufactured with less stringent processes. While the effects of incubating Zeonor with aqueous solutions over long time periods on the electrokinetic potential have been investigated [1], to the authors' knowledge, no previous results for the temporal dependence of the electrokinetic potential

Table 2
Comparison of electrokinetic-potential measurements for Zeonor from different studies. In [10], the reported data was taken after the solution and Zeonor substrate equilibrated for 4 h, so our data at $t = 4$ h is shown for comparison.

	Experiment	$\frac{\zeta}{pC}$ (mV)
Tandon et al. [10]	Current monitoring	−23.8
Tandon et al. [10]	Streaming potential	−20.7
This study	Streaming Potential (at $t = 4$ h)	−17.8

of Zeonor with high temporal resolution (12 min) have been reported. In Table 2, several reported values for the (phenomenologically defined) equilibrium electrokinetic potential of Zeonor are shown to be in good agreement. Meaningful comparison is challenging, however, since equilibrium is defined differently in each of the experiments.

The electrokinetic potential of silica did not show any pressure or time dependence, with a normalized time-averaged value of −25.8 mV in air at 0.47 atm (the normalized standard deviation of the time average was 3%, suggesting that the electrokinetic potential was constant). This agrees well with our measured value at 1 atm (−27.8 mV), and with previously published results [30,45–47].

We have previously postulated that the time dependence of the electrokinetic potential in hydrophobic substrates may be related to the nucleation and dissipation of nanobubbles at the fluid–solid interface [30]. Nanobubbles are gas bubbles of diameter on the order of 50–200 nm, which form at hydrophobic interfaces, and are classically predicted by the Young–Laplace equation to be highly unstable. They have been observed via AFM to form at water–hydrophobe interfaces [26,34,29,48–50], but not at hydrophilic interfaces [34], and, since they are thermodynamically unstable, they have a lifetime on the order of hours [27,28,26,29]. The presence of gas at the interface changes the fluid velocity boundary condition, and introduces an apparent slip [19]. For a given interfacial potential, ψ_0, slip leads to an increase in the electrokinetic potential, ζ, which can be estimated using the following expression in the Debye–Hückel, thin double layer limit [20].

$$\zeta = \psi_0\left(1 + \frac{b}{\lambda_D}\right) \tag{3}$$

Here, ζ is the measured electrokinetic potential, ψ_0 is the interfacial potential, b is the Navier slip length, and λ_D is the Debye length. Experiments [51] and MD simulations [52,53] have demonstrated the significance of slip in electrokinetic systems, though the phenomena is not well understood, and the effects of surface roughness and non-uniform surface conduction within thin double layers have been shown to be important, setting a limit to the effect of slip [54,55]. Since nanobubbles are unstable, their decay over time is expected to result in the reduction of the apparent electrokinetic potential.

While the origin of slip on hydrophobic substrates is unclear [19], slip has been shown to be modulated by the type of dissolved gas in solution [31]. In addition, the state of dissolved gases has been observed to affect the density of water near the fluid–solid interface [23]. Nanobubble thermodynamic stability is also expected to depend on the concentration of dissolved gas in the fluid [26,56], which depends on the pressure of gas in equilibrium with the fluid, as given by Henry's law.

$$P = k_H C \tag{4}$$

Here, C is the concentration of dissolved gas, k_H is the Henry coefficient for the particular fluid–gas system at a given temperature, and P is the partial pressure of the gas in equilibrium with the fluid. The dependence of electrokinetic potential equilibration kinetics on the ambient atmospheric pressure observed in this study is consistent with nanobubbles as a mechanism for introducing apparent slip, leading to an inflated electrokinetic potential. Reduced ambient pressure results in a lower dissolved gas concentration, faster dissolution of nanobubbles, and a more rapid approach to the equilibrium electrokinetic potential.

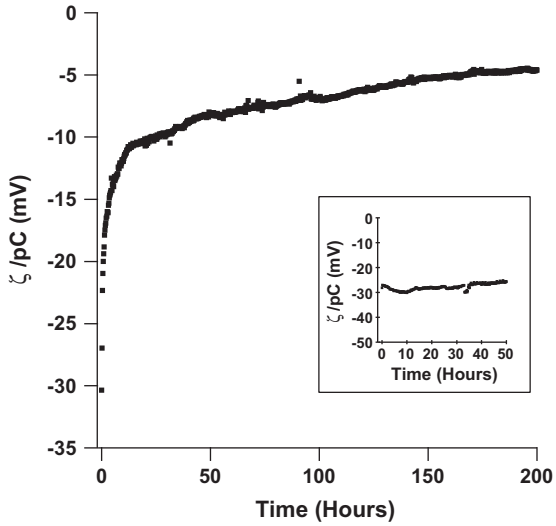

Fig. 3. ζ-potential measurement in Zeonor at 1 atm over a time period of 200 h. The Zeonor data shown is an average of two replicates. The inset shows the electrokinetic potential in silica over at time period of 50 h for comparison. Data shown is ζ normalized by $pC = -\log C$ (C is the counterion concentration in M) as a function of time for a Zeonor substrate. 1 mM, pH 7 phosphate buffer was the working solution.

4.2. Very-long-term behavior of ζ at atmospheric pressure

In order to better establish the equilibrium electrokinetic potential for the Zeonor–water interface in air at 1 atm, we conducted a long-term (200 h), phase-sensitive streaming potential experiment (Fig. 3). As was the case with the 20 h experiment, the magnitude of the normalized electrokinetic potential was initially high at ∼−30 mV. The electrokinetic potential continued to decrease beyond the value observed at 20 h, however, to −4.62 mV after 200 h. In comparison, the electrokinetic potential of the silica–water interface was constant over 50 h, with a normalized, time-averaged value of −27.8 mV and a standard deviation of 4%.

The temporal dependence of the electrokinetic potential at atmospheric pressure is characterized by an exponential decay with two time constants, one long and one short. The data in Fig. 2 was fit to exponential functions in order to determine the dependence of these time constants on ambient pressure (Table 3). As the ambient pressure is decreased, the long time constant decreases dramatically, while the short time constant is affected less. (The 0.74 and 0.47 atm cases were nearly the same.) In all cases, the electrokinetic potential approached nearly the same value at $t = \infty (\zeta_\infty/pC \sim -3$ mV). For the 0.47 and 0.74 atm cases, the long and short time constants are very similar to each other, indicating that those data may be well-described by an exponential decay with a single time constant.

Table 3
The sub-atmospheric data sets in Fig. 2, and the data in Fig. 3 were fit to double exponential functions ($\zeta = \zeta_\infty + \zeta_1 e^{-t/\tau_1} + \zeta_2 e^{-t/\tau_2}$, where ζ_1 and ζ_2 are fit parameters, τ_1 and τ_2 are the time constants, and ζ_∞ is the value of ζ at $t = \infty$), using a non-linear least-squares optimization. All fits had an R^2 value greater than 0.99.

Pressure (atm)	ζ_∞/pC mV	τ_1 h	τ_2h
1.00	−3.0	115.21	2.85
0.87	−4.4	4.23	1.91
0.74	−2.5	1.48	1.26
0.47	−3.8	1.99	1.96

The steady state is independent of pressure, but pressure regulates the kinetics of the approach to steady state. This suggests that lower ambient pressure results in a more rapid approach to steady state, rather than a change in the equilibrium electrokinetic potential. To the authors' knowledge, no previous data on the electrokinetic potential of Zeonor substrates after long-term equilibration with aqueous solution has been published. Mela et al. [1] showed that incubating a Zeonor substrate with phosphate buffer solution for 10 days, and then flushing with new solution, resulted in a slight increase in the electrokinetic potential. This is consistent with our observations, as flushing would likely expose Zeonor microchannels to air, resulting in a temporary increase in the electrokinetic potential.

4.3. Electrokinetic-potential hysteresis with dissolved gas concentration

Given the postulated role of nanobubbles in electrokinetic potentials of hydrophobic substrates, we expect that the observed pressure dependence of the electrokinetic potential of the Zeonor–water system is fundamentally due to the state of dissolved gases in solution. When the ambient pressure is decreased, a finite amount of time is required for the solution to come to equilibrium with the surrounding gas (Fig. 4). Using the data in Fig. 4 and a model for gas transfer kinetics, we calculated the dissolved O_2 concentration in the working solution as a function of time in each of our low-pressure experiments. The electrokinetic potential as a function of dissolved O_2 concentration is nearly the same for all of the sub-atmospheric pressures examined (Fig. 5). It decreases in magnitude approximately linearly with dissolved O_2 concentration until the normalized (with respect to the equilibrium concentration at 1 atm air pressure) concentration is ~0.9, at which point ζ is constant with further decrease in the O_2 content.

The collapse of data taken at different sub-atmospheric pressures shown in Fig. 5 suggests that the response of ζ to changes in dissolved gas content is relatively rapid as compared to the natural equilibration time of the electrokinetic potential seen at

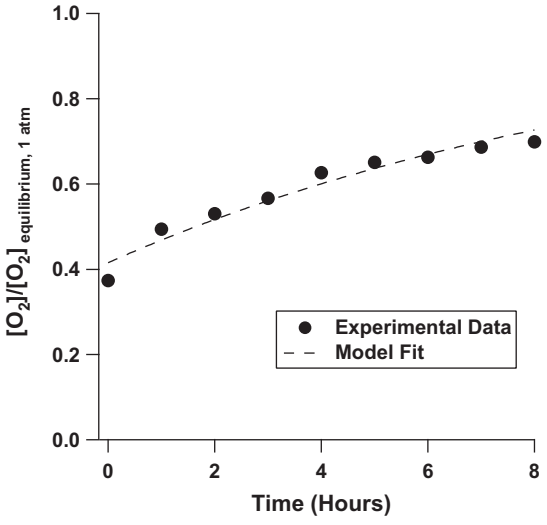

Fig. 4. Dissolved O_2 content in pH 7, 1 mM phosphate buffer as a function of time. The solution was first allowed to equilibrate at low pressure (0.47 atm) for 20 h. It was then removed from vacuum (returned to 1 atm ambient pressure), and the dissolved O_2 concentration was measured as a function of time. Data was fit to a model for oxygen transfer between air and solution based on first order kinetics, assuming a well-stirred solution in contact with an infinite reservoir of air, and equilibrium conditions defined by Henry's Law. The rate constant for O_2 entering solution was calculated from the fit to be $(10.5\ h)^{-1}$. Data shown is normalized by the dissolved O_2 content of a solution in equilibrium with air at 1 atm.

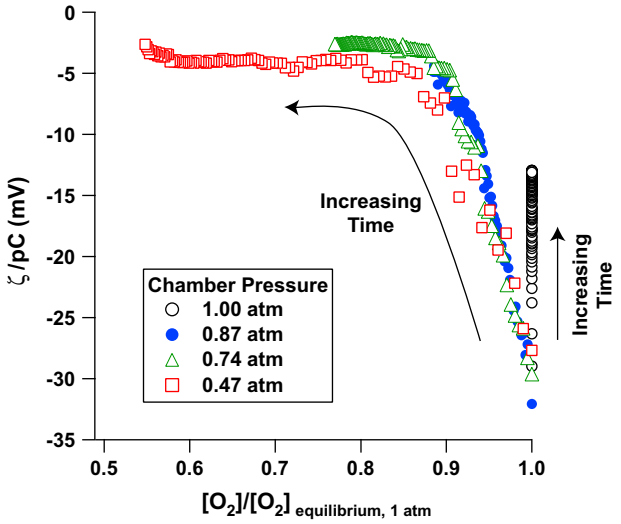

Fig. 5. The electrokinetic potential, ζ, normalized by pC = −log$C$ (C is the counterion concentration in M) as a function of dissolved O_2 concentration for several ambient pressures. Dissolved O_2 concentration as a function of time was calculated using the model and data described in Fig. 4. The points are evenly spaced in time, at 12 min intervals. Dissolved O_2 concentration is normalized by the dissolved O_2 content of a solution in equilibrium with air at 1 atm.

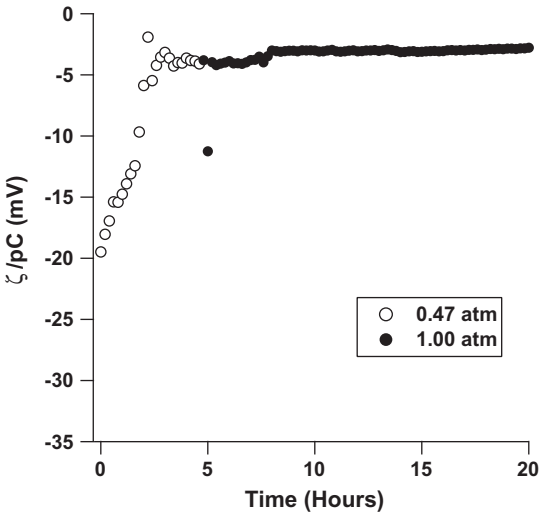

Fig. 6. The electrokinetic potential, ζ, normalized by pC = −log$C$ (C is the counterion concentration in M) as a function of time for a Zeonor substrate. 1 mM, pH 7 phosphate buffer was the working solution. The experiment was initiated at 0.47 atm ambient pressure, and the pressure was raised to 1 atm after 5 h.

atmospheric pressure. Thus, the timescales of the electrokinetic-potential decay associated with the sub-atmospheric pressures in Fig. 2 are expected to be more representative of the equilibration time of dissolved gas in the system. The faster approach to equilibrium seen at lower pressures is due to the faster decrease in dissolved gas content.

We also investigated whether the altered time dependence of the electrokinetic potential of the Zeonor–water interface at low ambient pressures is reversible by starting a phase-sensitive streaming potential experiment at low (0.47 atm) pressure, and then increasing the pressure to 1 atm after 5 h (Fig. 6). At the start of the experiment, the working solution was at equilibrium with air at atmospheric pressure, the pressure in the experimental chamber was lowered, and the streaming potential experiment was initiated immediately thereafter. The electrokinetic potential

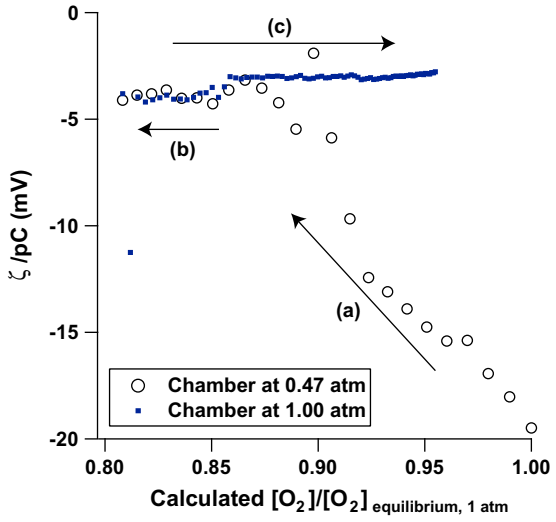

Fig. 7. The electrokinetic potential of a Zeonor substrate exhibits a type of hysteresis with changing dissolved gas conditions. The ζ/pC data from Fig. 6 is shown here as a function of dissolved O_2 concentration. The points are evenly spaced in time, at 12 min intervals. Dissolved O_2 concentration as a function of time was calculated using the model and data described in Fig. 4. (a) A solution that was in equilibrium with air at 1 atm is suddenly exposed to air at 0.47 atm. ζ/pC decreases in magnitude as the dissolved O_2 concentration decreases. (b) ζ/pC has stopped decreasing in magnitude, but the dissolved O_2 concentration continues to decrease. (c) The air in the chamber is returned to a pressure of 1 atm. The dissolved O_2 concentration increases, but ζ/pC does not change.

as a function of time is very similar to that seen in Fig. 2 for 0.47 atm, and the return to 1 atm pressure did not have an observable effect on the electrokinetic potential, as it remained constant across the changeover at 5 h. This, combined with the long-term experiment, suggests that the equilibrium electrokinetic potential is not a function of pressure in the observed range, though pressure affects the kinetics of equilibration.

Examination of the electrokinetic potential data in Fig. 6 as a function of dissolved O_2 content reveals a type of hysteresis (Fig. 7). When the ambient pressure is 0.47 atm, the electrokinetic potential magnitude decreases with decreasing solution O_2 concentration until it reaches the equilibrium value, as was the case in all of the sub-atmospheric experiments. Returning the ambient pressure to 1 atm results in the O_2 concentration increasing towards its original value. The electrokinetic potential magnitude, however, does not increase back to its original value, but rather remains constant with the increasing gas concentration.

Though the electrokinetic potential magnitude decreased with decreasing solution gas content, it stopped decreasing at a particular solution gas concentration. This is consistent with unstable nanobubbles that nucleate at the water–Zeonor interface upon replacing air in the capillary with aqueous solution, and that dissipate at a rate that depends on the amount of dissolved gas in solution. Once the electrokinetic potential has reached equilibrium (i.e. the nanobubbles have dissipated), increasing the ambient atmospheric pressure back to 1 atm may stabilize existing nanobubbles, but it is not expected to result in the formation of new ones. The air content in solution at most reaches the same value it was at the start, which is not sufficient to stabilize nanobubbles [26].

5. Conclusions

We have demonstrated that the kinetics governing equilibration of the electrokinetic potential of Zeonor microfluidic substrates are dependent on the ambient air pressure. Upon initial formation of the fluid–solid interface, Zeonor substrates have electrokinetic potential that is initially high in magnitude that ultimately decays to an equilibrium value. Across ambient air pressures ranging from 0.47 atm to 1 atm, the normalized electrokinetic potential tends to the same equilibrium value (−5 to −3 mV). The approach to equilibrium, however, is faster at lower ambient air pressures. In silica substrates, the electrokinetic potential does not change with time, or with ambient pressure. Once the electrokinetic potential has reduced in magnitude, increasing the ambient air pressure does not increase it again, suggesting hysteresis of the electrokinetic potential with solution dissolved gas content.

For hydrophobic substrates, in addition to pH, conductivity, temperature, etc., the electrokinetic potential must also be considered as a function of the history of the solution dissolved gas concentration. While the dependence of the electrokinetic potential on ambient pressure and ethanol–water solvent exchanges [30] suggest that the amount of dissolved gas in solution affects the electrokinetic potential, future work will involve investigating different types of dissolved gases. Carbon dioxide, for example, has anomalously high solubility owing to its ability to form hydrogen bonds with water, and it can react to form carbonic acid [57–59]. In addition, direct observation of nanobubble dynamics using AFM will help strengthen the putative link between nanobubbles and macroscopically observable electrokinetic phenomena.

Understanding the effect of the state of dissolved gases on electrokinetics impacts characterization of surface charge and slip at hydrophobic interfaces, as well as design and optimization of microfluidic devices fabricated from hydrophobic polymers. Since pressure, temperature, and solution components can all affect gas solubility, heat, flow, and solvent cycling may lead to unexpected variations in device performance.

Acknowledgments

We would like to acknowledge our funding sources: Sandia National Labs (DOE PECASE) and ACS-PRF. We would also like to thank Sharath K. Bhagavatula for his help in developing the phase-sensitive streaming potential techniques, as well as Abraham D. Stroock (School of Chemical and Biomolecular Engineering, Cornell University) Blake A. Simmons (Sandia National Labs) for useful discussions.

References

[1] P. Mela, A. van den Berg, Y. Fintschenko, E.B. Cummings, B.A. Simmons, B.J. Kirby, Electrophoresis 26 (2005) 1792–1799.
[2] H.A. Stone, A.D. Stroock, A. Ajdari, Annu. Rev. Fluid Mech. 36 (2004) 381–411.
[3] J.C. McDonald, D.C. Duffy, J.R. Anderson, D.T. Chiu, H. Wu, O.J.A. Schueller, G.M. Whitesides, Electrophoresis 21 (2000) 27–40.
[4] B.G. Hawkins, A.E. Smith, Y.A. Syed, B.J. Kirby, Anal. Chem. 79 (2007) 7291–7300.
[5] W. Schutzner, E. Kenndler, Anal. Chem. 64 (1992) 1991–1995.
[6] C. Werner, H. Korber, R. Zimmermann, S. Dukhin, H. Jacobasch, J. Colloid Interface Sci. 208 (1) (1998) 329–346.
[7] L.E. Locascio, C.E. Perso, C.S. Lee, J. Chromatogr. A 857 (1) (1999) 275–284.
[8] J. Caslavska, W. Thormann, J. Microcolumn Separat. 13 (2) (2001) 69–83.
[9] B.J. Kirby, E.F. Hasselbrink Jr., Electrophoresis 25 (2004) 203–213.
[10] V. Tandon, S.K. Bhagavatula, W.C. Nelson, B.J. Kirby, Electrophoresis 29 (2008) 1092–1101.
[11] W. Dickinson, Trans. Faraday Soc. 37 (1941) 140.
[12] K.G. Marinova, R.G. Alargova, N.D. Denkov, O.D. Velev, D.N. Petsev, I.B. Ivanov, R.P. Borwankar, Langmuir 12 (1996) 2045–2051.
[13] C.C. Ho, K. Ahmad, J. Colloid Interface Sci. 216 (1999) 25–33.
[14] A. Graciaa, P. Creux, C. Dicharry, J. Lachaise, J. Dispersion Sci. Technol. 23 (2002) 301–307.
[15] I. Ametov, C.A. Prestidge, J. Phys. Chem. B 108 (32) (2004) 12116–12122.
[16] J. Gaudioso, H.G. Craighead, J. Chromatogr. A 971 (1) (2002) 249–253.
[17] J. Kameoka, H.G. Craighead, H. Zhang, J. Henion, Anal. Chem. 73 (2001) 1935–1941.
[18] A. Tan, S. Benetton, J.D. Henion, Anal. Chem. 75 (2003) 5504–5511.

[19] E. Lauga, M.P. Brenner, H.A. Stone, Microfluidics: The No-Slip Boundary Condition, Handbook of Experimental Fluid Dynamics, Springer, New York, 2005.
[20] V. Tandon, B.J. Kirby, Electrophoresis 29 (2008) 1102–1114.
[21] S.I. Mamatkulov, P.K. Khabibullaev, RR. Netz, Langmuir 20 (2004) 4756–4763.
[22] A. Poynor, L. Hong, I.K. Robinson, S. Granick, Z. Zhang, P.A. Fenter, Phys. Rev. Lett. 97 (2006) 266101.
[23] D.A. Doshi, E.B. Watkins, J.N. Israelachvili, J. Majewski, PNAS 102 (27) (2005) 9458–9462.
[24] L.X. Dang, T. Chang, J. Phys. Chem. B 106 (2002) 235–238.
[25] R. Zangi, J.B.F.N. Engberts, J. Am. Chem. Soc. 127 (2005) 2272–2276.
[26] P. Attard, M.P. Moody, J.W.G. Tyrell, Physica A 314 (2002) 696–705.
[27] P. Attard, Langmuir 12 (1996) 1693–1695.
[28] P. Attard, Langmuir 16 (2000) 4455–4466.
[29] P. Attard, Adv. Colloid Interface Sci. 104 (2003) 75–91.
[30] V. Tandon, S.K. Bhagavatula, B.J. Kirby, Electrophoresis 30 (2009) 2656–2667.
[31] S. Granick, Y. Zhu, H. Lee, Nat. Mater. 2 (4) (2003) 221–227.
[32] L. Meagher, V.S.J. Craig, Langmuir 10 (1994) 2736–2742.
[33] J. Mahnke, J. Stearnes, R.A. Hayes, D. Fornasiero, J. Ralston, Phys. Chem. Chem. Phys. 1 (1999) 2793–2798.
[34] N. Ishida, T. Inoue, M. Miyahara, K. Higashitani, Langmuir 16 (2000) 6377–6380.
[35] X.H. Zhang, X.D. Zhang, S.T. Lou, Z.X. Zhang, J.L. Sun, J. Hu, Langmuir 20 (2004) 3813–3815.
[36] R.F. Considine, R.A. Hayes, R.G. Horn, Langmuir 15 (1999) 1657–1659.
[37] W.M. Haynes (Ed.), CRC Handbook of Chemistry and Physics, 91 ed., CRC Press, 2010.
[38] E.L. Cussler, Diffusion – mass transfer in fluid systems, Cambridge University Press, Cambridge, United Kingdom, 1984.
[39] P. Han, D.M. Bartels, J. Phys. Chem. 100 (1996) 5597–5602.
[40] B.J. Kirby, D.S. Reichmuth, R.F. Renzi, T.J. Shepodd, B.J. Wiedenman, Lab Chip 5 (2005) 184–190.
[41] B. Ilic, D. Czaplewski, P. Neuzil, T. Stanczyk, J. Blough, G.J. Maclay, J. Mater. Sci. 38 (2000) 3447–3457.
[42] R.J. Hunter, Zeta Potential in Colloid Science, Academic Press, London, 1981.
[43] Brian J. Kirby, Micro- and Nano Scale Fluid Mechanics: Transport in Microfluidic Devices, Cambridge University Press, New York, NY, 2010.
[44] B.J. Kirby, E.F. Hasselbrink Jr., Electrophoresis 25 (2004) 187–202.
[45] P.J. Scales, F. Grieser, T.W. Healy, Langmuir 8 (1992) 965–974.
[46] M. Kosmulski, E. Matijevic, Langmuir 8 (1992) 1060–1064.
[47] J.E. Dickens, J. Gorse, J.A. Everhart, M. Ryan, J. Chromatogr. B 657 (1994) 401–407.
[48] S. Lou, J. Gao, X. Xiao, X. Li, G. Li, Y. Zhang, M. Li, J. Sun, X. Li, J. Hu, Mater. Charact. 48 (2002) 211–214.
[49] J.W.G. Tyrrell, P. Attard, Phys. Rev. Lett. 87 (17) (2001) 176104.
[50] J.W.G. Tyrrell, P. Attard, Langmuir 18 (2002) 160–167.
[51] N.V. Churaev, J. Ralston, I.P. Sergeeva, V.D. Sobolev, Adv. Colloid Interface Sci. 96 (2002) 265–278.
[52] L. Joly, C. Ybert, E. Trizac, L. Bocquet, Phys. Rev. Lett. 93 (2004) 257805.
[53] C.I. Bouzigues, P. Tabeling, L. Bocquet, Phys. Rev. Lett. 101 (2008) 114503.
[54] T.M. Squires, Phys. Fluids 20 (2008) 092105.
[55] A.S. Khair, T.M. Squires, Phys. Fluids 21 (2009) 042001.
[56] M.P. Brenner, D. Lohse, Phys. Rev. Lett. 101 (2008) 214505.
[57] H. Sato, N. Matubayasi, M. Nakahara, F. Hirata, Chem. Phys. Lett. 323 (2000) 257–262.
[58] G.K. Anderson, J. Chem. Thermodyn. 35 (2003) 1171–1183.
[59] A. Khan, J. Mol. Struct. (Thermochem) 664-665 (2003) 237–245.